Silicalite-1 Growth from Clear Solution: Effect of Alcohol Identity and Content on Growth Kinetics

Chil-Hung Cheng and Daniel F. Shantz*

Department of Chemical Engineering, Texas A&M University, College Station, Texas 77843-3122

Received: May 11, 2005; In Final Form: August 17, 2005

In situ small-angle X-ray scattering (SAXS) is used to investigate the influence of alcohol identity and content on silicalite-1 growth from clear solutions at 368 K. Several tetraalkyl orthosilicates ($Si(OR)_4$, R = Me, Pr, and Bu) are used to synthesize silicalite-1 from clear solution mixtures comparable to those previously investigated (i.e. 1:0.36:20 TEOS:TPAOH:H_2O (TEOS = tetraethyl orthosilicate; TPAOH = tetrapropylammonium hydroxide), 368 K). All TPAOH−organosiloxane mixtures studied form silica nanoparticles after aging at room temperature for 24 h. Full-profile fitting analysis of the SAXS data indicates the particles are ellipsoidal and is inconsistent with the presence of "nanoslabs" or "nanoblocks". Synthesis using TEOS as the silica source have an induction period of approximately 7.5 h and a growth rate of 1.90 ± 0.10 nm/h at 368 K. Changing the silica source to tetramethyl orthosilicate (TMOS) does not change the induction period; however the particle growth rate is decreased to 1.65 ± 0.09 nm/h at 368 K. Variable-temperature SAXS measurements for syntheses with TEOS and TMOS show the activation energy for silicalite-1 growth is 60.0 ± 2.9 and 73.9 ± 2.8 kJ/mol, respectively, indicating the alcohol identity does influence the growth rate. By mixing tetrapropyl orthosilicate (TPOS) with TEOS (1.6:1.0 molar ratio) as the silica source, the precursor solution shows a shorter induction period (6.0 h) and a faster particle growth rate (2.16 ± 0.06 nm/h). The alcohol identity effect is more pronounced when other organocations (e.g. alkyltripropylammonium cations) are used to make silicalite-1 at 368 K. Removing ethanol from the precursor solution decreases the induction period to approximately 4.5 h and increases the particle growth rate to 2.99 ± 0.13 nm/h. Mixtures with 2 equiv of ethanol have an induction period and particle growth rate of 6.0 h and 2.04 ± 0.03 nm/h, respectively. The results demonstrate the alcohol identity and content influence silicalite-1 growth kinetics. One possible explanation is varying the alcohol identity and content changes the strength of the hydrophobic hydration of the structure-directing agent and the water−alcohol interaction, resulting in less efficient interchange between clathrated water molecules and solvated silicate species.

Introduction

Zeolites are widely used in adsorption, ion-exchange processes, and heterogeneous catalysis.[1−4] It is this (and potentially other applications) that spurs the intense research effort into understanding their nucleation and growth. Silicalite-1, the all-silica form of ZSM-5,[5] is one of the most widely studied zeolite systems.[6−45] The nucleation and growth of silicalite-1, particularly from "clear solution" synthesis mixtures containing only tetrapropylammonium hydroxide TPAOH, tetraethyl orthosilicate (TEOS), and water, have been investigated using a battery of methods including nuclear magnetic resonance spectroscopy (NMR),[9−11] dynamic light scattering (DLS),[23−25,27,31−36] and small-angle X-ray/neutron scattering (SAXS/SANS).[12−18,37,38,42−45] Silicalite-1 nucleation and crystallization kinetics are highly dependent on temperature,[37,46] organocation identity,[18,47,48] silica source and content,[24,26,49] alkalinity of the solution,[14] and the presence of alkali cations.[50] Furthermore, the organocation's properties also influence zeolite formation, for example, the hydrophobicity,[51,52] the ability to form van der Waals contact with silicate species,[9,11] and the geometry of the organocation.[47] A point significant to this investigation is that the role/influence of the alcohol generated by organosiloxane hydrolysis has not been studied, and it has generally been assumed to have little or no influence on the growth process.[7]

The particle size is highly dependent on the silica source and concentration.[24−26,49] Silica sources that have been investigated can be classified into two types: monomeric and polymeric. The typical example of the former is tetraethoxysilane (TEOS) and those for the latter would be silicic acid, fumed silica (Cab-O-Sil), and Ludox (colloidal silica). According to work by Persson and co-workers,[26] changing the silica source from TEOS to Ludox has several outcomes. These include that the particle size after room-temperature aging is larger, the induction period of the crystallization process increases, the particle growth rate increases slightly, the particle size of the final material is much larger than samples made with TEOS (400 nm vs 95 nm), and the particle polydispersity increases. To explain these results, the authors suggested that the colloidal silica particles are coated with TPA cations, preventing the dissolution of silica and resulting in a longer induction period. The authors also stated the increase in polydispersity is due to the silica source being polymeric in nature. Similar results were obtained by Mintova and Valtchev using transmission-type DLS (scattering angle ~ 173°)[24] and by Li et al. using a two-stage crystallization synthesis method studied with DLS, Raman spectroscopy, and scanning electron microscopy (SEM).[49] Mintova and Valtchev

* To whom correspondence should be addressed. Phone: (979) 845-3492. Fax: (979) 845-6446. E-mail: Shantz@che.tamu.edu.

10.1021/jp0524633 CCC: $30.25
Published on Web 09/27/2005

reported a slower crystallization rate when changing the silica source from TEOS to Ludox or Cab-O-Sil. Mintova and Valtchev claimed this is due to the dissolution of the polymeric silica and its subsequent repolymerization during zeolite formation but did not address the role of TPA cations during the process. All of these reports show the silica source influences the particle size, growth kinetics, and polydispersity, etc.

Syntheses employing monomeric silica sources such as TEOS lead to 4 equiv of alcohol as a byproduct. This corresponds to an approximately 28 wt % ethanol solution content for the mixture 1:0.36:20 TEOS:TPAOH:H_2O. Surprisingly few works have investigated the alcohol's role (if any) in zeolite nucleation and growth. The zeolite community has generally assumed it is a spectator. Persson et al. have reported that the zeolite growth rate decreases with increasing ethanol content, while Cundy et al. reported that the zeolite growth rate decreases when a large excess of ethanol was added ($EtOH:SiO_2 > 20$).[7,26] No explanation was given for these results.

Previous studies show that water−alcohol mixtures exhibit several nonidealities.[53,54] These include large-magnitude enthalpies and entropies of mixing, an abnormally large magnitude of the excess heat capacity both in water-rich and ethanol-rich regions under room temperature, and a relatively small decrease in the partial molar volume. These are all attributed to the enhancement of the water clathrate structure upon alcohol addition and that the alcohol occupies either framework or interstitial positions in the clathrate structure.[55] On the other hand, the interaction between water molecules and the alkyl groups of tetraalkylammonium cations results in the formation of a clathrate water sphere around the cation, referred to as hydrophobic hydration.[54] The clathrate water network is further reinforced as the alkyl groups are changed from methyl to butyl groups.[54]

These seemingly subtle points may in fact be crucial to understanding the nucleation and growth of silicalite-1 from clear solution. It has been postulated that displacement of the orgranocation's hydration sphere by small silicate species is an essential step in zeolite nucleation.[9,11] This process should, in principle, be influenced by alcohol. By contrast, the silicate speciation literature, most notably work by Kinrade et al.,[56,57] has argued that the organocations solvate the silicate anions, essentially the opposite viewpoint. Knight has also reported that there is a substantial enhancement of the cubic octamer upon methanol addition.[58] As such the speciation equilibrium is altered due to the alcohol identity and content. While many researchers, including those involved with the silicate speciation studies above, caution extrapolating room-temperature equilibrium measurements to events at synthesis conditions (higher *T*, nonequilibrium),[59] determining how alcohols influence the growth kinetics of silicalite-1 from clear solutions should illuminate this issue.

To our knowledge there is no study published investigating how the alcohol generated by organosiloxane hydrolysis influences growth kinetics of silicalite-1 from clear solutions. This point motivates the current work that attempts to answer the following questions*: what is the influence of the alcohol identity and alcohol concentration on silicalite-1 growth kinetics from clear solutions at 368 K?* With the help of in situ SAXS measurements, we quantitatively demonstrate the effect of the alcohol identity and content on silicalite-1 growth kinetics.

Experimental Section

Investigated Structure-Directing Agent (SDA) and Silanes. Tetrapropylammonium hydroxide (TPAOH, Alfa Aesar, 40 wt % in aqueous solution) was used as received. Alkyltripropylammonium cations ($R_1N(C_3H_7)_3^+OH^-$, R_1 = Me, Et, Bu, and Pe) were synthesized via alkylation of tripropylamine with the appropriate alkyl halide, recrystallized, and ion-exchanged as reported previously.[60] Tetramethyl orthosilicate (TMOS, Aldrich, 98%), tetraethyl orthosilicate (TEOS, Fluka, > 99%), tetrapropyl orthosilicate (TPOS, Aldrich, 95%), and tetrabutyl orthosilicate (TBOS, Aldrich, 97%) were used as received.

Zeolite Synthesis. Unless noted otherwise, syntheses were of composition $1:0.36:20:4\ SiO_2:R_1N(C_3H_7)_3^+[OH^-]:H_2O:R_2OH$ (R_2 = Me, Et, Pr, and Bu). A representative synthesis is as follows: 9 g of TEOS was added to 7.9 g of TPAOH. This mixture was stirred vigorously for 30 min, and 10.81 g of water was then added. The mixture was then aged for 24 h while mixing at room temperature. Then half of the solution was placed in a screw cap Teflon container and heated at 368 K until the solution became opaque on the basis of visual inspection. The solids were collected by centrifugation, washed with deionized water, dried, and characterized by powder X-ray diffraction (PXRD). The other half of the solution was used for in situ SAXS measurements. For samples prepared with various ethanol contents, a high-vacuum manifold was used to remove the ethanol generated by organosiloxane hydrolysis at room temperature. The ethanol and water removed were trapped in a vacuum trap that was submerged in a liquid nitrogen bath. This step was sustained until half of the solution volume was left. Additional water and ethanol (if needed) were subsequently added to make up the water lost during the evaporation.

Analytical Methods. PXRD measurements were performed on a Bruker AXS D8 powder diffractometer (Cu Kα radiation) in reflection mode from $2\theta = 4$ to 40° with a step size of 0.03° and 2 s/step. Field-emission scanning electron microscopy (FE-SEM) measurements were performed using a Zeiss Leo-1530 microscope operating at 1−10 kV. The microscope employs a GEMINI electron optical column with a Schottky-type field emitter, single condenser, crossover-free beam path, large specimen chamber with two chamber ports for energy-dispersive spectrometry (EDS) or wavelength-dispersive spectrometry (WDS) adaptation, four accessory ports on the chamber and three on the door, a fail-safe vacuum system, and digital image storage and processor.

The in situ SAXS experiments were performed on a Bruker NanoSTAR system with a Nonius rotating anode (FR591) and a copper target (1.5417 Å). The anode was operated at 45 kV and 90 mA. The X-ray beam was paralleled by a cross-coupled Göbel mirror and collimated by three pinholes (750, 400, and 1000 μm in order). The scattering intensity was measured on a two-dimensional multiwire Hi-STAR detector, and the residual direct beam was blocked by a beam stop. The detector was located 22 and 64 cm away from the sample, respectively, corresponding to a q range of 0.05−0.7 and 0.02−0.3 $Å^{-1}$ ($q = 4\pi \sin(\theta)/\lambda$; θ is half of the scattering angle, and λ is the wavelength of the incident beam). The exact sample-to-detector distance was determined using a silver behenate standard.

The in situ SAXS measurements were performed in an electrically heated stage containing a rotating round sample cell. The stage is very similar to that described by de Moor and coworkers.[18] Two clear mica disks (PSI, V1 grade, 15 mm in diameter, 0.15 mm in thickness) were used as windows, with spacing provided by a Teflon ring (McMaster-Carr Co., thickness, 0.5 mm). Cell heating was provided using two cartridge heaters (Omega Engineering Co., CIR-1014/120V) and the cell temperature was measured by a K-type thermocouple (Omega Engineering, unsheathed T/C) and controlled by a solid-state

relay temperature controller (Omega Engineering, CN76031). The in situ measurements were performed at 368 K, and the sampling time was 1.5 h during the reaction. The heating stage was mounted in an Anton Paar HR-PHK sample chamber, and the whole system was purged with helium (>99.99%) several times and then operated under vacuum (0.1 mbar). The scattered intensity of the particles was calculated on the basis of using water (room temperature and 368 K individually) as the reference material for the background subtraction in data analysis.[12,14] For obtaining the transmission coefficient of the sample, a piece of glassy carbon was inserted into the beam path as a second specimen after each measurement and was taken every three measurements. The transmission coefficients were almost identical during the process of the hydrothermal reaction. Because of the pinhole configuration on the SAXS instrument, no de-smearing procedure was required prior to data analysis.

The scattering data were analyzed using the program GNOM to determine the pair distance distribution function (PDDF),[61] which is based on the inverse Fourier transform method (IFT).[62−66] For data during the induction period, the particle diameter was obtained using the optimized perceptual criteria introduced by Svergun[61] as well as the Guinier approximation.[67] The radius of gyration obtained from the Guinier approximation is calculated assuming a spherical particle geometry. The values obtained from both approaches were almost identical. For scattering patterns measured following the induction period the particle size distribution was determined to be bimodal in nature. The diameter of the larger particles was determined from the Guinier approximation, and the particle diameter of the smaller particles was determined from the optimized perceptual criteria within the smaller guessing value ranges. The theoretical fitting matched the experimental scattering data in the high-q range for this optimized guessing value. However, the low-q range data cannot be described using just the small particle population. The growth rate during the crystallization period is determined from the particle diameter as a function of the synthesis duration using linear regression.

Results

Alcohol Identity. The initial work explored the syntheses of silicalite-1 using different silanes. All organosiloxanes can be used to make silicalite-1 at 368 K on the basis of the PXRD results shown in Figure 1. The PXRD peaks of silicalite-1 using TPOS as the silica source are narrower compared with the other three samples, indicating the particles are larger. The FE-SEM images are consistent with this. The particles of silicalite-1 using TPOS as the silica source are approximately 300 nm in size, larger than those of the other silica sources. Twinned crystals are also observed in the TPOS−silicalite-1 synthesis.[26,68,69] The particle shape of silicalite-1 using the other silica sources is spherical and the particle surface is not smooth, consistent with our previous work.[60] The different morphology and larger particle size of TPOS−silicalite-1 are surprising; given it is not observed for samples made using TBOS, it is likely not due to the use of a two-phase mixture, but rather appears to be unique to samples made in the presence of propanol. A more detailed explanation for this result is currently under investigation. Syntheses using TPOS or TBOS resulted in two-phase solutions due to the limited miscibility of propanol or butanol in water, which is generated from the hydrolysis of the corresponding silane. Given this, the SAXS results below focus on TEOS, TMOS, and TEOS/TPOS mixtures that are all one-phase solutions after room-temperature aging. Also, given that the major focus of this investigation is how the alcohol identity/content influences nucleation and growth, the results are structured around these points, and nucleation and growth in the systems are discussed together.

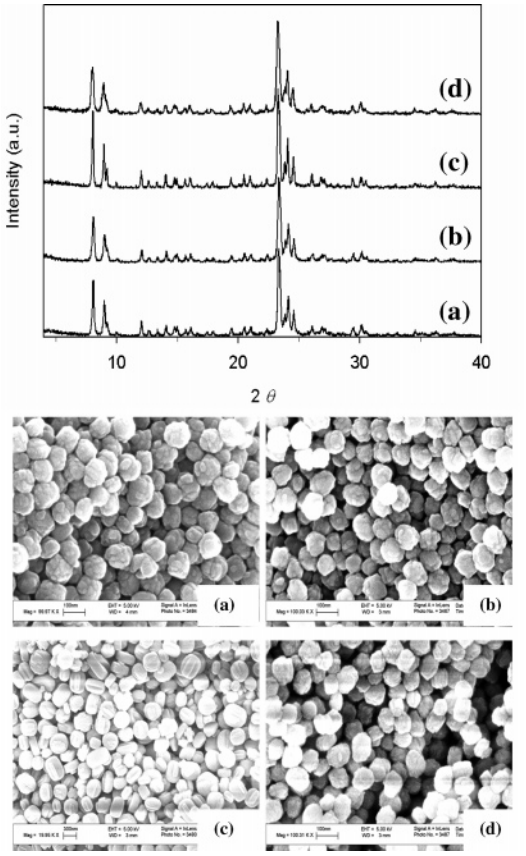

Figure 1. PXRD (top) and (bottom) FE-SEM images of silicalite-1 prepared with the composition of 1:0.36:20 organosiloxane:TPAOH:H_2O at 368 K for 1 week: (a) tetramethyl orthosilicate (TMOS); (b) tetraethyl orthosilicate (TEOS); (c) tetrapropyl orthosilicate (TPOS); (d) tetrabutyl orthosilicate (TBOS). The scale bar for a, b, and d is 100 nm, and the scale bar for c is 300 nm.

Growth Kinetics using TEOS. Although the growth kinetics of the TEOS−silicalite-1 system have been extensively studied,[20,21,24,26,31−34] in order to provide a direct comparison in the current work, the growth kinetics are revisited here at 363 and 358 K using in situ SAXS. Given the clear presence of particle−particle interactions (i.e. a clear maximum in the log−log plot of I versus q), the values obtained from the Guinier and IFT analyses are approximate, although they still lead to clear trends and conclusions. Figures 2 and 3 show the time-resolved scattering patterns of the solution 1:0.36:20 TEOS:TPAOH:H_2O at 363 and 358 K. The scattering patterns have a slope of −2 in the high-q range, identical with that of the same solution studied at 368 K, showing that the particles are nonspherical. Detailed analysis of the full scattering profile is problematic given the nonspherical shape of the particles as well as clear particle−particle interactions (i.e. $S(q) \neq 1$). This makes quantitative analysis of the scattering patterns ambiguous given the lack of analytical expressions for structure factors of nonspherical particles.[46] Full-profile fitting analyses of the scattering curve after room-temperature aging neglecting the structure factor effects are included in the Supporting Information and are consistent with either a cylindrical or ellipsoidal geometry. These results are consistent with most of the previous work in the literature[37,43−45,60] but are inconsistent with the presence of "nanoslabs" or "nanoblocks".[20,21,29,30,70−73] The lack of oscillations at high-q values indicates a degree of polydis-

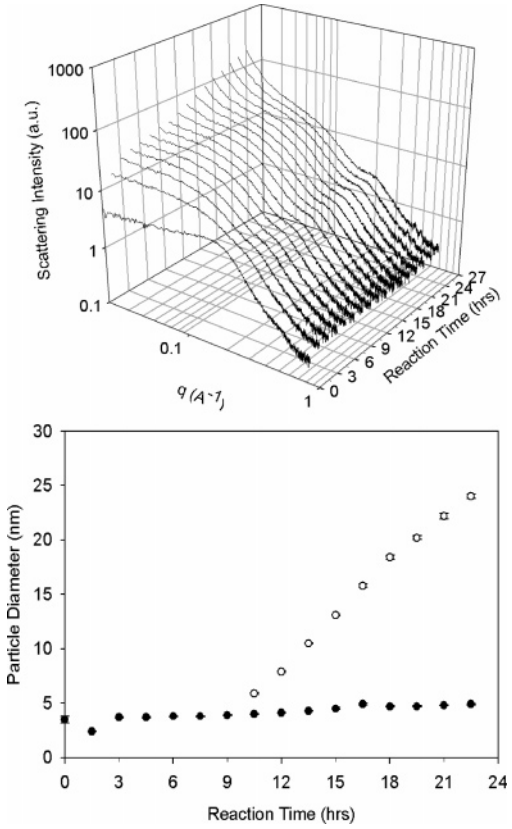

Figure 2. (Top) Time-resolved SAXS scattering patterns of 1:0.36:20 TEOS:TPAOH:H_2O at 363 K. (Bottom) Plot of particle size versus reaction time.

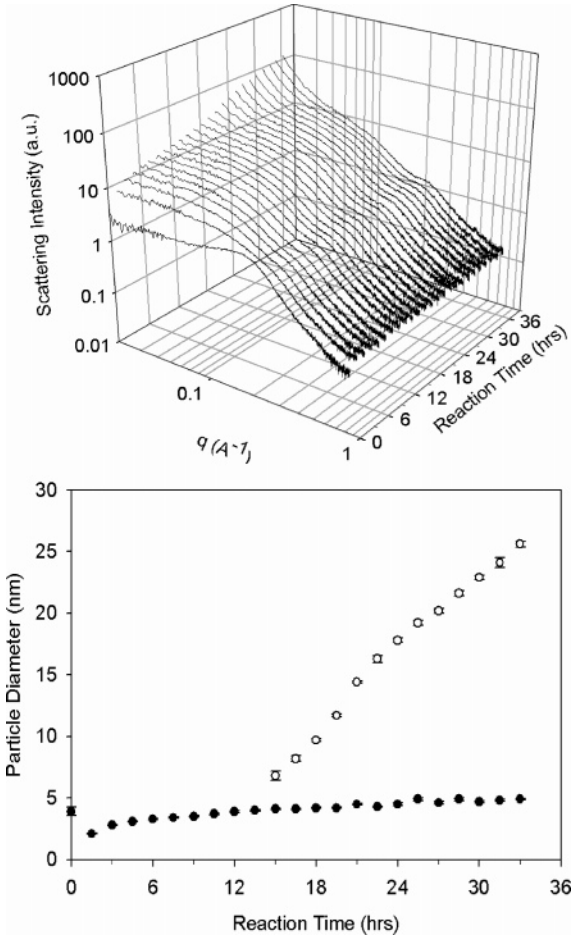

Figure 3. (Top) Time-resolved SAXS scattering patterns of 1:0.36:20 TEOS:TPAOH:H_2O at 358 K. (Bottom) Plot of particle size versus reaction time.

persity (or the absence of a sharp change in electron density at the particle−solution interface); however, full-profile fitting would be necessary to quantify this. The IFT analyses indicate a relatively small degree of polydispersity. The clear discrepancy of the full-profile fitting and the experimental scattering curve in the range of $q \leq 0.3$ Å^{-1} is due to neglecting particle−particle interactions. Ongoing work in our laboratory is exploring various full-profile analysis schemes and will be reported elsewhere. As observed in our previous work, there is an induction period, during which only the primary particles exist. After the induction period a second, larger, particle population emerges, resulting in a bimodal size distribution. The induction time and heating duration until observing Bragg diffraction peaks for silicalite-1 at 363 and 358 K are 10.5 and 15.0 h and 22.5 and 33.0 h, respectively. On the basis of the results presented here, whether the larger particles are silicalite-1 when they are less than 20−25 nm in size cannot be concluded. Ongoing work is studying this issue and will be reported elsewhere. During the induction period, the particle diameter decreases to 2 nm in the initial 1.5 h and then gradually grows to 4 nm. These 4 nm particles are present throughout crystallization on the basis of DLS and GNOM analysis.[60] The larger particles, first observed at the end of the induction period, grow from 4 to 24 nm in 13.5 h at 363 K and from 4 nm to approximately 26 nm in 19.5 h at 358 K, resulting in growth rates of 1.55 ± 0.03 and 1.10 ± 0.03 nm/h, respectively. Combined with our previous results at 368 K,[60] an Arrhenius plot is shown in Figure 4. The activation energy of silicalite-1 growth using TEOS as the silica source is obtained from the slope using linear regression ($r^2 = 0.98$) and is 60.0 $\pm$ 2.9 kJ/mol. This value is comparable with previous results.[7,17,27,36,74]

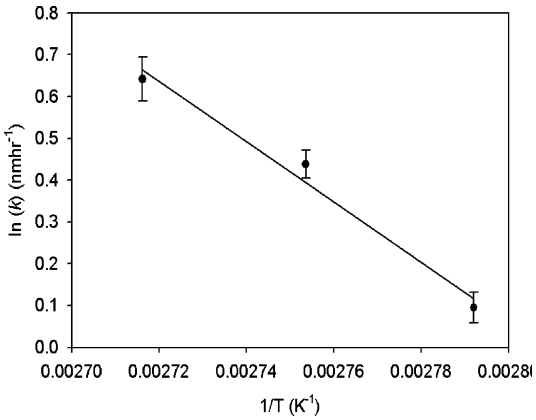

Figure 4. Arrhenius plot of the silicalite-1 growth kinetics (1:0.36:20 TEOS:TPAOH: H_2O) at 368, 363, and 358 K.

Growth Kinetics Using TMOS. Figure 5 shows the time-resolved SAXS scattering patterns of silicalite-1 at 368 K synthesized using TMOS. The slope in the Porod regime of each scattering curve is approximately −2.2. The induction time and heating duration until observing Bragg diffraction peaks are 7.5 and 19.5 h correspondingly. The induction period is comparable to that for syntheses with TEOS at 368 K, but the growth rate is slower. During the induction period the primary particles, initially 4 nm in diameter after room temperature aging, decrease to 2 nm in the first 1.5 h of heating and gradually increase to 4 nm. The larger particles grow from 4 to 27 nm over a period of 13.5 h in coexistence with the 4 nm primary particles. The particle growth rate is 1.65 ± 0.09 nm/h. Figures 6 and 7 show the time-resolved SAXS scattering patterns of

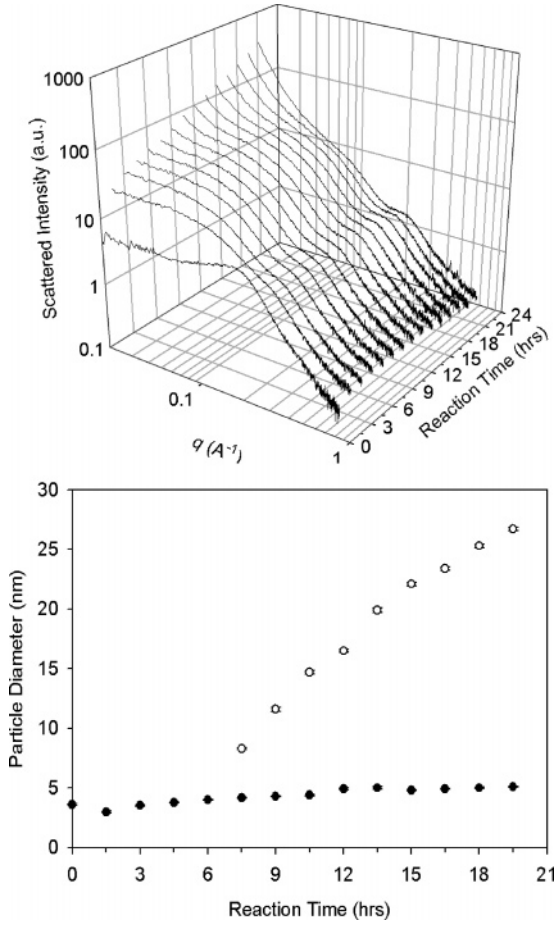

Figure 5. (Top) Time-resolved SAXS scattering patterns of 1:0.36:20 TMOS:TPAOH:H_2O at 368 K. (Bottom) Plot of particle size versus reaction time.

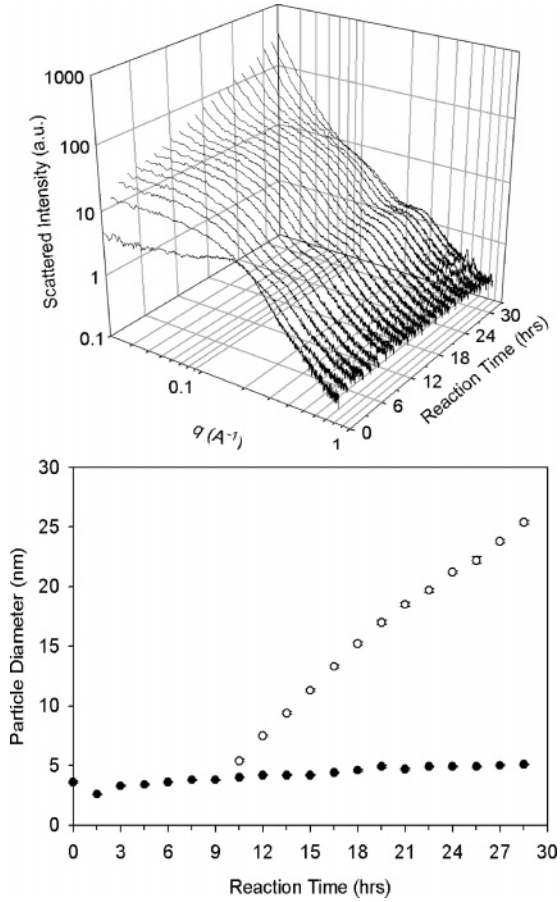

Figure 6. (Top) Time-resolved SAXS scattering patterns of 1:0.36:20 TMOS:TPAOH:H_2O at 363 K. (Bottom) Plot of particle size versus reaction time.

silicalite-1 mixtures at 363 and 358 K using TMOS. At both temperatures the primary particles are nonspherical on the basis of the slope in the Porod regime, and the particle size distribution during growth is bimodal with the primary particle size of 4 nm for both cases. The induction period has increased to 10.5 and 16.5 h, and the reaction time for the appearance of the Bragg diffraction peaks becomes 28.5 and 40.5 h, respectively. The growth rate of the larger particles decreases to 1.11 ± 0.03 nm/h at 363 K and 0.84 ± 0.02 nm/h at 358 K. These results are used to generate the Arrhenius plot shown in Figure 8, from which the activation energy is determined to be 73.9 ± 2.8 kJ/mol ($r^2 = 0.98$).

Several points are observed when changing the silica source from TEOS to TMOS (Table 1). First, a faster particle growth rate for TEOS solutions at three different reaction temperatures, indicating the alcohol identity does affect the growth kinetics of silicalite-1. Second, both crystallization reactions are likely surface reaction limited;[17,26,27,36,37] however, the energy barrier of the reaction is lower for the ethanol-containing solution. Third, the primary particle sizes after room-temperature aging, during the induction period, and the number density of particles are not sensitive to the alcohol identity. Fourth, the induction period duration does not appear to be highly sensitive to the alcohol identity. The third point indicates the pH (organocation/Si, OH/Si) is the main factor in controlling the primary particle size and the number density of the precursor particles. Given the difference of the hydrophobicity between ethanol and methanol, we hypothesize the growth of silicalite-1 particles *in the presence of a fixed amount of alcohol* is more favorable as the alcohol becomes more hydrophobic. This hypothesis is further investigated by changing the silica source to a mixture of TPOS with TEOS.

Mixtures Containing TEOS/TPOS. Being unable to obtain a one-phase solution by using TPOS as the silica source, syntheses were performed with TEOS/TPOS in different ratios while keeping the total silica concentration constant. Within a fairly broad range of TEOS/TPOS ratios (0.5−4.9) homogeneous clear solutions are formed after mixing for 2−3 days at room temperature. On the basis of PXRD results, all the precursor solutions form silicalite-1 after heating at 368 K within 1 day (Supporting Information). Figure 9 shows the in situ SAXS scattering patterns for a 0.38:0.62:0.36:20 TEOS:TPOS:TPAOH:H_2O solution at 368 K. The slope in the high-q range is approximately −2.1. The induction period and the heating period until silicalite-1 Bragg diffraction peaks are observed have decreased to 6 and 15 h, respectively, displaying a faster growth rate as compared to syntheses with TEOS. During the induction period, the particle diameter increases from 3 to 4 nm. The 4 nm particles exist during the crystallization step and gradually grow to 5 nm. The larger particles grow from 4 to 26 nm in 10.5 h, leading to a particle growth rate of 2.16 ± 0.06 nm/h. Figure 10 summarizes the silicalite-1 growth rates at 368 K and shows that during the crystallization stage the growth rate is in the order propanol + ethanol > ethanol > methanol. This is consistent with the growth rate increasing as the alcohol becomes more hydrophobic and is consistent with the SEM image shown in Figure 1.

Ethanol Content. Figure 11 shows the time-resolved SAXS scattering patterns of the solution 1:0.36:20 TEOS:TPAOH:H_2O

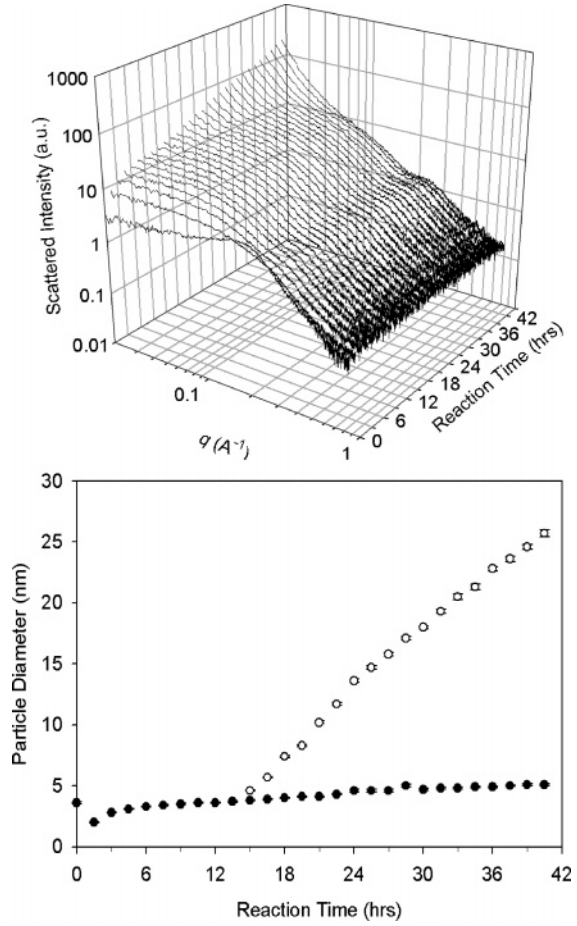

Figure 7. (Top) Time-resolved SAXS scattering patterns of 1:0.36:20 TMOS:TPAOH:H_2O at 358 K. (Bottom) Plot of particle size versus reaction time.

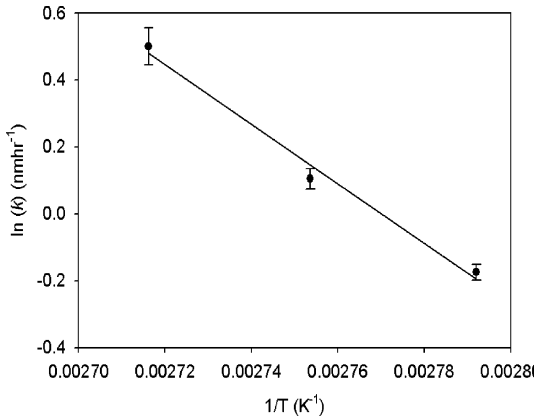

Figure 8. Arrhenius plot of the silicalite-1 growth kinetics (1:0.36:20 TMOS:TPAOH:H_2O) at 368, 363, and 358 K.

at 368 K, where the ethanol was removed. The solution also possesses particle−particle interactions prior to heating, as indicated by the maximum at 0.16 $Å^{-1}$. The position of the maxima has shifted to higher q values, indicating the particle size after removing ethanol is smaller. The slope of the scattering patterns in the high-q range is approximately −2.1. The induction period is 4.5 h, and silicalite-1 Bragg diffraction peaks are observed after 10.5 h of heating. These results show that the induction period is shorter and the growth rate is faster without ethanol. During the induction period the particle diameter changes from 3 to 4 nm. The larger particles grow from 4 to 25 nm over a period of 7.5 h, resulting in a growth rate of 2.99 ± 0.13 nm/h. Mixtures were also studied containing

TABLE 1: Growth Kinetics Summary for 1:0.36:20 $Si(OR)_4$:TPAOH:H_2O (R = $-CH_3$, $-CH_2CH_3$)[a]

	TMOS	TEOS
primary particle diameter after RT aging (nm)	3.6 ± 0.1	3.4 ± 0.1
scattered intensity at zero angle, $I(0)$	5.14 (368 K)	5.95 (368 K)
	4.04 (363 K)	4.18 (363 K)
	2.97 (358 K)	2.21 (358 K)
368 K		
induction period (h)	7.5−9.0	6.0−7.5
primary particle size during induction (nm)	4.0	4.1
growth rate (nm/h)	1.65 ± 0.09	1.9 ± 0.1
363 K		
induction period (h)	9.0−10.5	9.0−10.5
primary particle size during induction (nm)	3.8	4.0
growth rate (nm/h)	1.11 ± 0.03	1.55 ± 0.03
358 K		
induction period (h)	13.5−15.0	13.5−15.0
primary particle size during induction (nm)	3.8	4.0
growth rate (nm/h)	0.84 ± 0.02	1.1 ± 0.04
activation energy (kJ/mol)	73.9 ± 2.8	60.0 ± 2.9

[a] Silica sources: TMOS = tetramethyl orthosilicate; TEOS = tetraethyl orthosilicate.

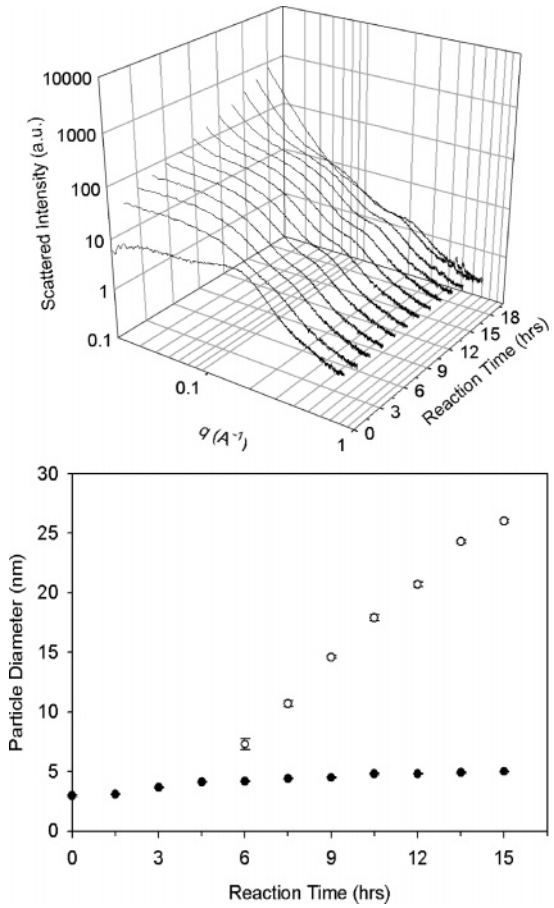

Figure 9. (Top) Time-resolved SAXS scattering patterns of (x TEOS + y TPOS): 0.36 TPAOH: 20 H_2O at 368 K where $x = 0.38$ and $y = 0.62$; (Bottom) Plot of particle size versus reaction time.

2 equiv of ethanol. The SAXS data and particle growth profile of that mixture are shown in Figure 12. The particle size distribution is still bimodal with the primary particles 4 nm in diameter. The induction period is 6.0 h, and the time for the appearance of Bragg diffraction peaks is 15.0 h of heating, leading to a growth rate of 2.04 ± 0.03 nm/h, slower than in the absence of ethanol. Figure 13 summarizes the growth rates of silicalite-1 particles at 368 K with three alcohol contents during the crystallization stage and clearly demonstrates that

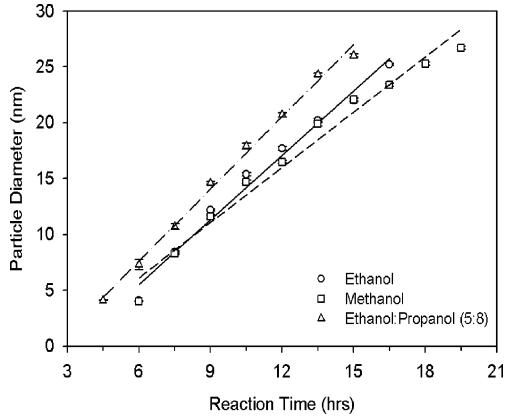

Figure 10. Alcohol identity effect on the silicalite-1 growth rate at 368 K.

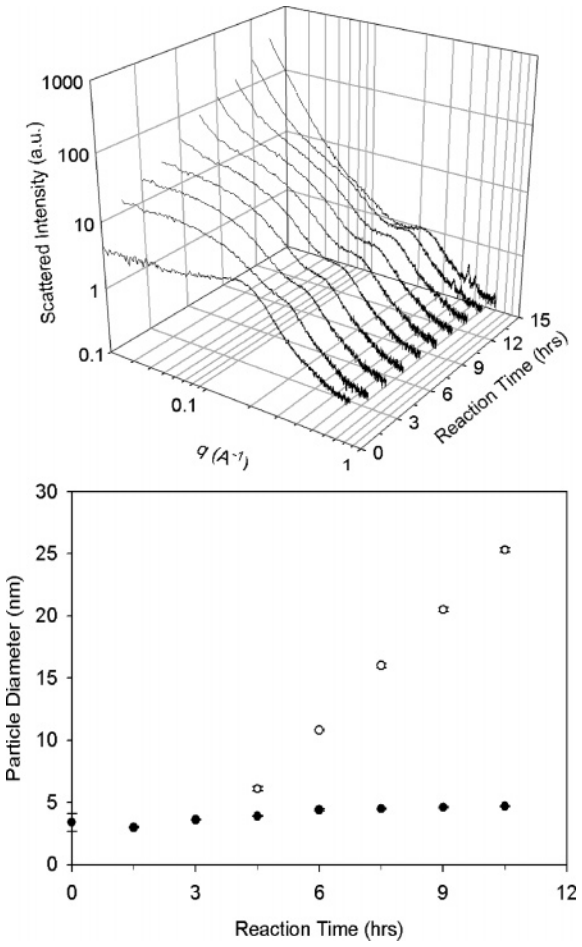

Figure 11. (Top) Time-resolved SAXS scattering patterns of 1:0.36:20 TEOS:TPAOH:H_2O at 368 K after removing the ethanol. (Bottom) Plot of particle size versus reaction time.

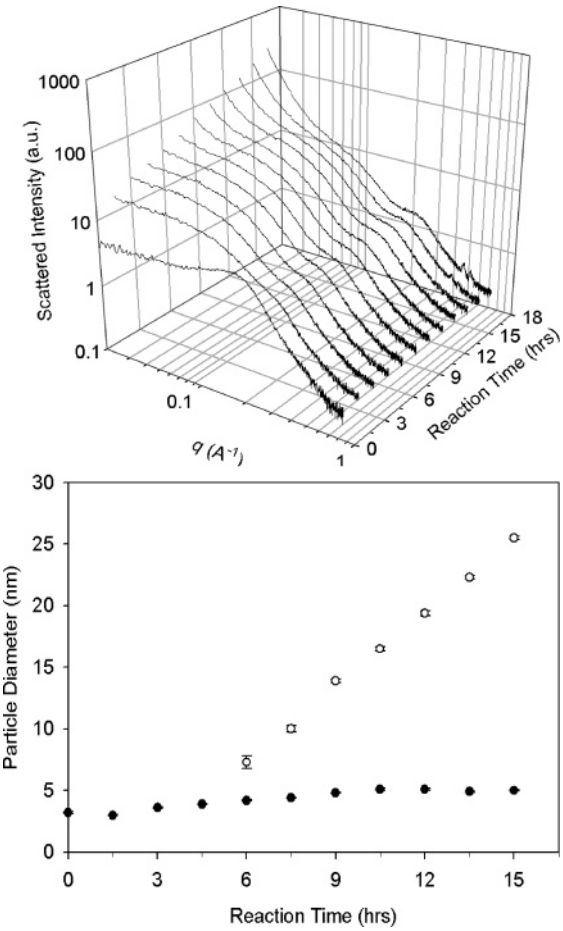

Figure 12. (Top) 368 K time-resolved SAXS scattering patterns of 1:0.36:20 TEOS:(TPA)OH:H_2O with 2 equiv of ethanol added after ethanol removal. (Bottom) Plot of particle size versus reaction time.

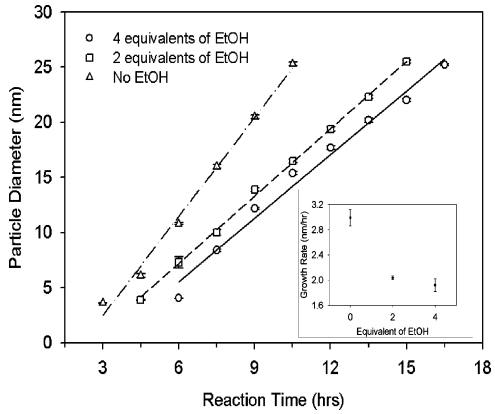

Figure 13. Silicalite-1 growth kinetics at 368 K as a function of ethanol content. The inset is a plot of the particle growth rate versus the ethanol content.

the alcohol content also influences the crystallization rate. These results are consistent with the work by Persson and co-workers and Cundy,[7,26] showing that the particle growth rate is decreased as the ethanol content increases. Possible reasons for this are given below (vide infra).

Other SDAs and the Influence of Alcohol. The results above indicate that the TPA−silicalite-1 synthesis is sensitive to the alcohol identity. This was further investigated by studying silicalite-1 growth kinetics using alkyltripropylammonium (RPr_3N^+) cations as the SDA with different organosiloxanes. We have previously reported that these SDAs will direct the formation of silicalite-1 at 368 K using TEOS.[60] Silica rapidly precipitates from solutions of 1:0.36:20 TMOS:methyltripropylammonium hydroxide:H_2O at room temperature. The precipitate is amorphous silica on the basis of PXRD (Supporting Information). After removing the precipitates, the clear solution was heated at 368 K for 7 days and silicalite-1 was formed (Supporting Information). The same result was obtained when methyltripropylammonium hydroxide was replaced with pentyltripropylammonium hydroxide, except that the precipitate forms over the course of several hours. These results show that the stability of the primary particles is influenced by changing the organosiloxane from TEOS to TMOS (i.e. the alcohol identity).

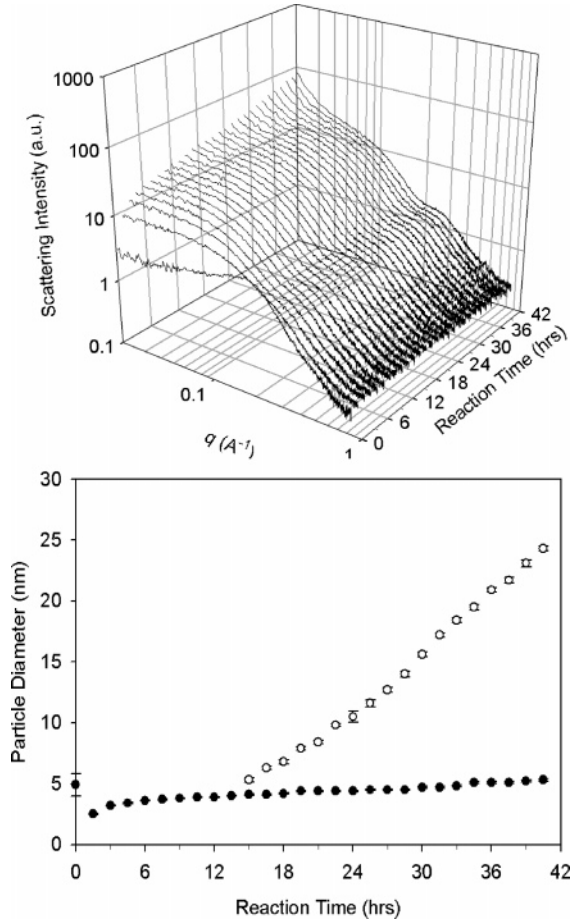

Figure 14. (Top) time-resolved SAXS scattering patterns of 1:0.36:20 TMOS:ethyltripropylammonium hydroxide:H_2O at 368 K. (Bottom) Plot of particle size versus reaction time.

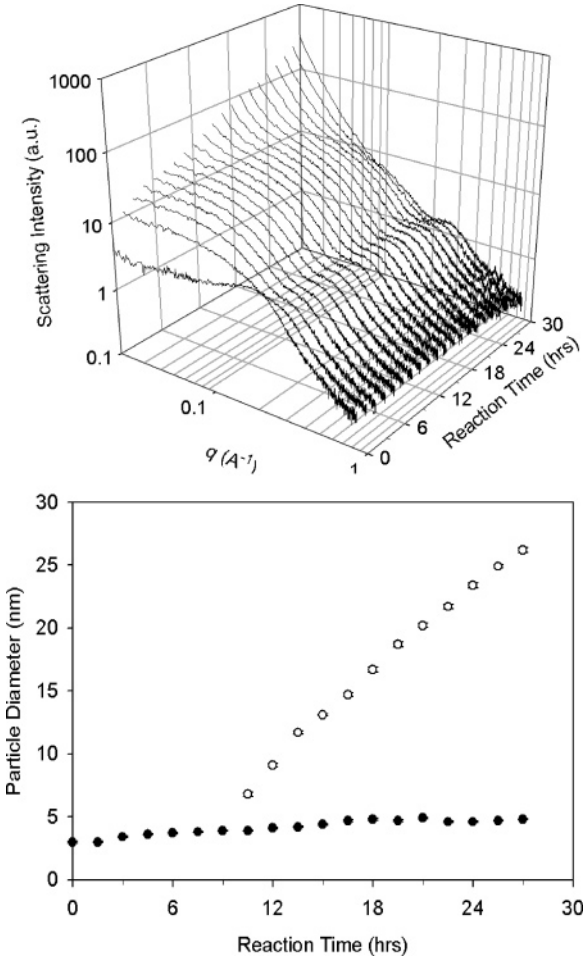

Figure 15. (Top) time-resolved SAXS scattering patterns of 1:0.36:20 TMOS:butyltripropylammonium hydroxide:H_2O at 368 K. (Bottom) Plot of particle size versus reaction time.

Syntheses performed with ethyltripropylammonium hydroxide ($(C_2H_5)N^+(C_3H_7)_3OH^-$) and butyltripropylammonium hydroxide ($(C_4H_9)N^+(C_3H_7)_3OH^-$) using TMOS as the silica source result in homogeneous transparent solutions after room-temperature aging for 24 h. The precursor solutions form silicalite-1 after heating at 368 K on the basis of PXRD data (Supporting Information). Figures 14 and 15 show the time-resolved scattering patterns of silicalite-1 made using $EtPr_3N^+$ and $BuPr_3N^+$ cations in the presence of TMOS. The slope of the scattering patterns in the high-q range is approximately -2. The induction periods for $BuPr_3N^+$ and $EtPr_3N^+$ are 10.5 and 13.5 h, respectively, and Bragg diffraction peaks in the Porod regime are not observed until after 27.0 and 40.5 h of heating, respectively. As summarized in Table 2 with the comparison of our previous study,[60] the induction periods are longer and growth rates are slower when the silica source is changed to TMOS for both cases. During the induction period, for the $EtPr_3N^+$ mixture the primary particle diameter decreases to 2.5 nm in the first 1.5 h of hydrothermal reaction and then gradually increases to 4 nm, whereas for the $BuPr_3N^+$ mixture the primary particles decrease to 3 nm in the first 1.5 h of hydrothermal reaction and then gradually grow to 4 nm. The growth rates for the $EtPr_3N^+$ and $BuPr_3N^+$ systems are 0.76 ± 0.02 and 1.21 ± 0.03 nm/h, respectively. These values are smaller than those of silicalite-1 made using these SDAs in the presence of TEOS. On the basis of the above results, the hydrophobicity of the alcohol does affect the silicalite-1 growth kinetics with the trend of MeOH < EtOH < 1-PrOH. Further, these differences are more pronounced when cations beside TPA are used to synthesize silicalite-1.

Discussion

The results presented above show how alcohol identity and content influence the growth kinetics of silicalite-1 from clear solutions at 368 K. As summarized in Tables 1 and 2, the growth kinetics are sensitive to the alcohol identity as changing the silica source from TEOS to TMOS leads to slower growth rates for TPA−silicalite-1 but substantial changes for the other organocations studied above. The silicalite-1 crystallization growth rate using TEOS as the silica source is larger than those using TMOS. The results show that silicalite-1 growth is faster as the alcohol becomes more hydrophobic. This observation is further supported by silicalite-1 samples grown in TEOS/TPOS mixtures. The effect of ethanol content on the silicalite-1 growth rate is also studied, showing the growth rate increases as the ethanol content decreases. These results show that even for a system as robust as TPA−silicalite-1, that growth is not independent of the alcohol identity or content.

The effect of the alcohol identity, however, is much more pronounced when silicalite-1 is made in the presence of other organocations. This is most dramatically manifested by the inability to stabilize silica nanoparticles when methyltripropylammonium hydroxide and pentyltripropylammonium hydroxide are used as the SDAs and TMOS as silica source. Our previous work shows very different results when TEOS is employed instead of TMOS.[60] The particle growth rates using ethyltripropylammonium hydroxide and butyltripropylammonium hydroxide as the SDAs and TMOS as silica source are also shown to

TABLE 2: Comparison of 1:0.36:20 $Si(OR)_4$:R′N$(C_3H_7)_3^+OH$:H_2O (R′ = Et, Bu and R = Me, Et)[a]

	organocation $EtN(C_3H_7)_3^+OH$		organocation $BuN(C_3H_7)_3^+OH$	
	TMOS	TEOS[59]	TMOS	TEOS[59]
primary particle diameter after RT aging (nm)	4.9 ± 0.1	3.4 ± 0.1	3.0 ± 0.1	3.4 ± 0.1
scattering intensity at zero angle, $I(0)$	2.23	7.0	3.01	6.6
368 K				
induction period (h)	13.5−15.0	10.5−12.0	9.0−10.5	7.5−9.0
primary particle size during induction (nm)	4.0	4.1	4.0	4.1
growth rate (nm/h)	0.76 ± 0.02	0.8 ± 0.02	1.21 ± 0.03	1.56 ± 0.1

[a] Silica sources: TMOS = tetramethyl orthosilicate; TEOS = tetraethyl orthosilicate.

be slower than those of using TEOS as the silica source correspondingly.

These results demonstrate two points: (1) tetrapropylammonium hydroxide is a robust and efficient structure-directing agent regardless of the organosiloxane source, and (2) the diameter (about 4 nm) and the number density of the primary particles (which is proportional to $I(0)$) are almost independent of the alcohol identity. Point 1 is likely due to both the geometry of TPA and the C/N^+ ratio. This point has been described by Zones and Davis.[47,48,52,75] The number density of the primary particle is found to decrease during crystallization for both silica sources and three investigated temperatures, consistent with literature results.[37] On the basis of the above results, the growth rate is slower when methanol is present in the precursor solutions compared to ethanol or propanol. One possible reason is due to the alcohol modifying the interaction strength between the silicate, alcohol molecules, water molecules, and organocations. It is well-known that over the whole composition range the water−alcohol mixtures exhibit several nonideal properties.[53,76] All of these properties are attributed to the enhancement of the water clathrate structure when alcohol is added as the solute. An important difference between the two alcohols is that methanol is claimed to occupy water framework positions in the clathrate structure, whereas ethanol favors interstitial positions in the clathrate structure. This results in the methanol−water mixture having a higher temperature of maximum density (TMD), which is a metric of the balance between structural expansion and break down as the temperature is raised.[55] Furthermore, the interaction between alcohol and water molecules is stronger for methanol than ethanol, on the basis of the smaller magnitude of the second virial coefficient for methanol.[76] With respect to the interaction between water molecules and tetraalkylammonium cations, the interaction results in the formation of a clathrated water sphere around the cation (hydrophobic hydration).[54] The clathrated water network is further reinforced as the alkyl groups are changed from methyl to butyl group. Burkett and Davis proposed the effective interchange of the clathrate water molecules and silicate species is one of the factors in formation of silicalite-1.[9−11] In this context the slower growth rate might be attributed to the stronger interaction between methanol and water molecules when methanol is present, resulting in a slower exchange rate of solvated silicate species and clathrate water molecules around the organocation molecules. This picture is also consistent with the increased silicalite-1 growth rate as the alcohol content is decreased (Figures 11 and 12).

The results for $MePr_3N^+$ and $PePr_3N^+$ as the SDAs and TMOS as the silica source are the most surprising, since changing ethanol to methanol results in the inability of these cations to stabilize colloidal silica particles. Also of note is that the formation rate of the amorphous silica precipitate for $MePr_3N^+$ (<3 min) is much faster than that of $PePr_3N^+$ (2−3 h). The instability of the colloidal silica particles due to changing the alcohol was not expected and could be attributed to the poor solvation ability of silicate species and organocations in methanol−water mixture.[76] The silicalite-1 "colloidal precursor" particles have recently been identified to possess a core−shell structure with organocations in the shell domain.[43,44] The solvated organocations may serve as an external scaffold to stabilize the encapsulated silica particles.[56] In going from ethanol to methanol the solvation layer around the organocations could be weakened which would subsequently destabilize the silica nanoparticles. Given that the stability of the particles made using TMOS appears dependent on the organocation identity, it cannot currently be ruled out that organocation self-association plays a role in this process as all solutions are approximately 1 M in organocation. Ongoing work is exploring this in more detail.

Conclusion

The SAXS results reported here quantitatively demonstrate that the growth kinetics of silicalite-1 using TPAOH as the SDA is influenced by the alcohol identity and content. Full-profile fitting analysis of the SAXS data indicates the particles are ellipsoidal and is inconsistent with the presence "nanoslabs" or "nanoblocks". Using mixtures of TPOS and TEOS as the silica source also enhances the growth kinetics of silicalite-1. The results indicate that for a fixed alcohol content a more hydrophobic alcohol increases silicalite-1 growth kinetics. Additionally, removing the ethanol generated from the hydrolysis of TEOS also enhances the growth kinetics. The variation of ethanol content within the water-rich range has only a minor effect on growth kinetics, consistent with previous work. Silicalite-1 syntheses employing other organocations such as alkyltripropylammonium cations are strongly sensitive to the alcohol identity. Syntheses using methyltripropylammonium hydroxide ($(CH_3)N(C_3H_7)_3^+OH^-$) or pentyltripropylammonium hydroxide ($(C_5H_{11})N(C_3H_7)_3^+OH^-$) as the SDAs and TMOS as the silica source lead to precipitates, showing that the presence of methanol results in the inability to stabilize colloidal silica particles in these mixtures. These results show that the alcohol does influence zeolite growth. One possible explanation is the alteration of the interchange efficiency between the clathrated water molecules around the organocations and the solvated silicate species in these mixtures as the alcohol is changed.

Acknowledgment. The authors acknowledge financial support from Texas A&M University and SABIC USA Inc. The SAXS instruments were purchased from funds obtained under National Science Foundation (NSF) Grant CTS-0215838. The authors acknowledge the X-ray Diffraction Facility at Texas A&M University for access to the XRD and SAXS instruments and the Microscopy and Imaging Center (MIC) at Texas A&M for access to the FE-SEM instrumentation. The FE-SEM acquisition was supported by the NSF under Grant No. DBI-0116835.

Supporting Information Available: Full-profile fitting of in situ SAXS pattern of the precursor solution with composition

of 1:0.36:20 TEOS:TPAOH:H_2O after heating for 4.5 h, full-profile fitting of the precursor solution with composition of 1:0.36:380 TEOS:TPAOH:H_2O after aging at room temperature for 24 h, PXRD patterns of syntheses mixtures with composition 1:0.36:20 organosiloxane:TPAOH:H_2O (organosiloxane = TMOS, TEOS, TPOS, and TBOS) and with composition *x*:*y*:0.36:20 TEOS:TPOS:TPAOH:H_2O (while $x = 0.83$ to 0.33, and $y = 0.17$ to 0.67) performed in Teflon containers at 368 K for 1 week, PXRD patterns of the precipitates collected from the mixtures with composition 1:0.36:20 TMOS:methyltripropylammonium hydroxide:H_2O and with composition 1:0.36:20 TMOS:pentyltripropylammonium hydroxide:H_2O performed in Teflon containers at room temperature for 24 h and the powder collected after the remaining solution reacted at 368 K for 7 days, PXRD patterns of the solid collected from the mixture with composition 1:0.36:20 TMOS:ethyltripropylammonium hydroxide:H_2O and with composition 1:0.36:20 TMOS:butyltripropylammonium hydroxide:H_2O performed in a Teflon container at 368 K for 7 days. This material is available free of charge via the Internet at http://pubs.acs.org.

References and Notes

(1) *Catalysis and Zeolites: Fundamentals and Applications*; Weitkamp, J., Puppe, L., Eds.; Springer: Berlin, New York, 1999.

(2) Barrer, R. M. *Hydrothermal Chemistry of Zeolites*; Academic Press: London, 1982.

(3) Bein, T. *Chem. Mater.* **1996**, *8*, 1636−1653.

(4) Breck, D. W. *Zeolite Molecular Sieves: Structure, Chemistry and Use*; Wiley: New York, 1974.

(5) Flanigen, E. M.; Bennett, J. M.; Grose, R. W.; Cohen, J. P.; Patton, R. L.; Kirchner, R. M.; Smith, J. V. *Nature* **1978**, *271*, 512−516.

(6) Cundy, C. S.; Lowe, B. M.; Sinclair, D. M. *J. Cryst. Growth* **1990**, *100*, 189−202.

(7) Cundy, C. S.; Lowe, B. M.; Sinclair, D. M. *J. Chem. Soc., Faraday Discuss.* **1993**, *95*, 235−252.

(8) Cundy, C. S.; Forrest, J. O.; Plaisted, R. J. *Microporous Mesoporous Mater.* **2003**, *66*, 143−156.

(9) Burkett, S. L.; Davis, M. E. *J. Phys. Chem.* **1994**, *98*, 4647−4654.

(10) Burkett, S. L.; Davis, M. E. *Chem. Mater.* **1995**, *7*, 1453−1463.

(11) Burkett, S. L.; Davis, M. E. *Chem. Mater.* **1995**, *7*, 920−928.

(12) de Moor, P.-P. E. A.; Beelen, T. P. M.; Komanschek, B. U.; Diat, O.; van Santen, R. A. *J. Phys. Chem. B* **1997**, *101*, 11077−11086.

(13) de Moor, P.-P. E. A.; Beelen, T. P. M.; van Santen, R. A. *Microporous Mater.* **1997**, *9*, 117−130.

(14) de Moor, P.-P. E. A.; Beelen, T. P. M.; van Santen, R. A. *J. Appl. Crystallogr.* **1997**, *30*, 675−679.

(15) de Moor, P.-P. E. A.; Beelen, T. P. M.; Komanschek, B. U.; van Santen, R. A. *Microporous Mesoporous Mater.* **1998**, *21*, 263−269.

(16) de Moor, P.-P. E. A.; Beelen, T. P. M.; van Santen, R. A.; Tsuji, K.; Davis, M. E. *Chem. Mater.* **1999**, *11*, 36−43.

(17) de Moor, P.-P. E. A.; Beelen, T. P. M.; van Santen, R. A. *J. Phys. Chem. B* **1999**, *103*, 1639−1650.

(18) de Moor, P.-P. E. A.; Beelen, T. P. M.; van Santen, R. A. *J. Phys. Chem. B* **2000**, *104*, 7600−7611.

(19) Kragten, D. D.; Fedeyko, J. M.; Sawant, K. R.; Rimer, J. D.; Vlachos, D. G.; Lobo, R. F.; Tsapatsis, M. *J. Phys. Chem. B* **2003**, *107*, 10006−10016.

(20) Kirschhock, C. E. A.; Ravishankar, R.; Van Looveren, L.; Jacobs, P. A.; Martens, J. A. *J. Phys. Chem. B* **1999**, *103*, 4972−4978.

(21) Kirschhock, C. E. A.; Ravishankar, R.; Jacobs, P. A.; Martens, J. A. *J. Phys. Chem. B* **1999**, *103*, 11021−11027.

(22) Kirschhock, C. E. A.; Buschmann, V.; Kremer, S.; Ravishankar, R.; Houssin, C. J. Y.; Mojet, B. L.; van Santen, R. A.; Grobet, P. J.; Jacobs, P. A.; Martens, J. A. *Angew. Chem., Int. Ed.* **2001**, *40*, 2637−2640.

(23) Mintova, S.; Olson, N. H.; Senker, J.; Bein, T. *Angew. Chem., Int. Ed.* **2002**, *41*, 2258−2561.

(24) Mintova, S.; Valtchev, V. *Microporous Mesoporous Mater.* **2002**, *55*, 171−179.

(25) Mintova, S.; Valtchev, V.; Bein, T. *Colloids Surf., A* **2003**, *217*, 153−157.

(26) Persson, A. E.; Schoeman, B. J.; Sterte, J.; Ottesstedt, J. E. *Zeolites* **1994**, *14*, 557−567.

(27) Schoeman, B. J.; Sterte, J.; Otterstedt, J. E. *Zeolites* **1994**, *14*, 568−575.

(28) Ravishankar, R.; Kirschhock, C. E. A.; Schoeman, B. J.; Vanoppen, P.; Grobet, P. J.; S., S.; Maier, W.; Martens, J. A.; De Schryver, F. C.; Jacobs, P. A. *J. Phys. Chem. B* **1998**, *102*, 2633−2639.

(29) Ravishankar, R.; Kirschhock, C. E. A.; Knops-Gerrits, P.-P.; Feijen, E. J. P.; Grobet, P. J.; Vanoppen, P.; De Schryver, F. C.; Miehe, G.; Fuess, H.; Schoeman, B. J.; Jacobs, P. A.; Martens, J. A. *J. Phys. Chem. B* **1999**, *103*, 4960−4964.

(30) Ravishankar, R.; Kirschhock, C. E. A.; Verspeurt, F.; Grobet, P. J.; Jacobs, P. A.; Martens, J. A. *J. Phys. Chem. B* **1999**, *103*, 4965−4971.

(31) Schoeman, B. J.; Regev, O. *Zeolites* **1996**, *17*, 447−456.

(32) Schoeman, B. J. *Microporous Mesoporous Mater.* **1997**, *9*, 267−271.

(33) Schoeman, B. J. *Zeolites* **1997**, *18*, 97−105.

(34) Schoeman, B. J. *Stud. Surf. Sci. Catal.* **1997**, *105*, 647−654.

(35) Schoeman, B. J. *Microporous Mesoporous Mater.* **1998**, *22*, 9−22.

(36) Twomey, T. A. M.; Mackay, M.; Kuipers, H. P. C. E.; Thompson, R. W. *Zeolites* **1994**, *14*, 162−168.

(37) Watson, J. N.; Iton, L. E.; Keir, R. I.; Thomas, J. C.; Dowling, T. L.; White, J. W. *J. Phys. Chem. B* **1997**, *101*, 10094−10104.

(38) Watson, J. N.; Brown, A. S.; Iton, L. E.; White, J. W. *J. Chem. Soc., Faraday Trans.* **1998**, *94*, 2181−2186.

(39) Yang, S.; Navrotsky, A. *Chem. Mater.* **2002**, *14*, 2803−2811.

(40) Yang, S.; Navrotsky, A.; Wesolowski, D.; Pople, J. A. *Chem. Mater.* **2004**, *16*, 210−219.

(41) Yang, S. Y.; Navrotsky, A. *Chem. Mater.* **2004**, *16*, 3682−3687.

(42) Iton, L. E.; Trouw, F.; Epperson, J. E.; White, J. W.; Henderson, S. J. *Langmuir* **1992**, *8*, 1045−1048.

(43) Fedeyko, J. M.; Vlachos, D. G.; Lobo, R. F. *Langmuir* **2005**, *21*, 5197−5206.

(44) Fedeyko, J. M.; Rimer, J. D.; Lobo, R. F.; Vlachos, D. G. *J. Phys. Chem. B* **2004**, *108*, 12271−12275.

(45) Rimer, J. D.; Vlachos, D. G.; Lobo, R. F. *J. Phys. Chem B* **2005**, *109*, 12762−12771.

(46) Pedersen, J. S. *Adv. Colloid Interface Sci.* **1997**, *70*, 171−210.

(47) Beck, L. W.; Davis, M. E. *Microporous Mesoporous Mater.* **1998**, *22*, 107−114.

(48) Goretsky, A. V.; Beck, L. W.; Zones, S. I.; Davis, M. E. *Microporous Mesoporous Mater.* **1999**, *28*, 387−393.

(49) Li, Q.; Mihailova, B.; Creaser, D.; Sterte, J. *Microporous Mesoporous Mater.* **2000**, *40*, 53−62.

(50) Goepper, M.; Li, H.-X.; Davis, M. E. *Chem. Commun.* **1992**, 1665−1666.

(51) Davis, M. E.; Lobo, R. F. *Chem. Mater.* **1992**, *4*, 756−768.

(52) Lobo, R. F.; Zones, S. I.; Davis, M. E. *J. Inclusion Phenom. Mol. Recognit. Chem.* **1995**, *21*, 47−78.

(53) Franks, F.; Ives, D. J. G. *Q. Rev. Chem. Soc.* **1966**, *20*, 1−44.

(54) Turner, J.; Soper, A. K. *J. Chem. Phys.* **1994**, *101*, 6116−6125.

(55) Dixit, S.; Crain, J.; Poon, W. C. K.; Finney, J. L.; Soper, A. K. *Nature* **2002**, *415*, 829−832.

(56) Kinrade, S. D.; Knight, C. T. G.; Pole, D. L.; Syvitski, R. T. *Inorg. Chem.* **1998**, *37*, 4272−4277.

(57) Kinrade, S. D.; Knight, C. T. G.; Pole, D. L.; Syvitski, R. T. *Inorg. Chem.* **1998**, *37*, 4278−4283.

(58) Knight, C. T. G. *Zeolites* **1989**, *9*, 448−450.

(59) Knight, C. T. G.; Syvitski, R. T.; Kinrade, S. D. *Stud. Surf. Sci. Catal.* **1995**, *97*, 483−488.

(60) Cheng, C. H.; Shantz, D. F. *J. Phys. Chem. B* **2005**, *109*, 13912−13920.

(61) Svergun, D. I. *J. Appl. Crystallogr.* **1992**, *25*, 495−503.

(62) Glatter, O. *J. Appl. Crystallogr.* **1977**, *10*, 415−421.

(63) Glatter, O. *J. Appl. Crystallogr.* **1979**, *12*, 166−173.

(64) Glatter, O. *J. Appl. Crystallogr.* **1980**, *13*, 7−11.

(65) Glatter, O. *J. Appl. Crystallogr.* **1980**, *13*, 577−584.

(66) Glatter, O.; Kratky, O. *Small Angle X-ray Scattering*; Academic Press: London, 1982.

(67) Guinier, A.; Fournet, G. *Small-Angle Scattering of X-rays*; Wiley: New York, 1955.

(68) Price, G. D.; Pluth, J. J.; Smith, J. V.; Bennett, J. M.; Patarin, J. *J. Am. Chem. Soc.* **1982**, *104*, 5971−5977.

(69) Hay, D. G.; Jaeger, H.; Wilshier, K. G. *Zeolites* **1990**, *10*, 571−576.

(70) Knight, C. T. G.; Kinrade, S. D. *J. Phys. Chem. B* **2002**, *106*, 3329−3332.

(71) Kirschhock, C. E. A.; Ravishankar, R.; Verspeurt, F.; Grobet, P. J.; Jacobs, P. A.; Martens, J. A. *J. Phys. Chem. B* **2002**, *106*, 3333−3334.

(72) Ramanan, H.; Kokkoli, E.; Tsapatsis, M. *Angew. Chem., Int. Ed.* **2004**, *43*, 4558−4561.

(73) Kirschhock, C. E. A.; Liang, D.; Aerts, A.; Aerts, C. A.; Kremer, S. P. B.; Jacobs, P. A.; Tendeloo, G. V.; Martens, J. A. *Angew. Chem., Int. Ed.* **2004**, *43*, 4562−4564.

(74) Feoktistova, N. N.; Zhdanov, S. P. *Zeolites* **1989**, *9*, 136−139.

(75) Helmkamp, M. M.; Davis, M. E. *Annu. Rev. Mater. Sci.* **1995**, *25*, 161−192.

(76) Franks, F.; Desnoyers, J. E. In *Water Science Reviews*; Franks, F., Ed.; Plenum: London, 1983; pp 171−232.